Egypt. J. Phys. **Vol. 51,** pp. 57-71 (2023)

Egyptian Journal of Physics

https://ejphysics.journals.ekb.eg/

Zinc Oxide Nanoparticles: Green Synthesis, Characterization, Photocatalysis, and Antibacterial Activity

Hussein S. A[1], Walaa Fouad[1], H. S. Wasly[2], Bahig A. El-Deeb[3], M.S. Abd El-sadek[*1]

[1]*Nanomaterials Lab., Physics Department, Faculty of Science, South Valley University, Qena, 83523, Egypt.*

[2]*Mining, Metallurgy and Petroleum Engineering Department, Faculty of Engineering, Al-Azhar University, Qena 83513, Egypt*

[3]*Department of Botany, Faculty of Science, Sohag University, Sohag, Egypt*

Abstract

The present work employs Ocimum Basilicum extract as a bio-reducing and a capping agent to synthesize zinc oxide nanoparticles (ZnO NPs) at different temperatures (30 ^{o}C, ^{6}0 ^{o}C, and 90 ^{o}C) in an efficient, simple, and environmentally friendly method (green synthesis), as well as their use in treating wastewater and antibacterial activity. The samples have a hexagonal structure confirmed by the X-ray Diffraction (XRD), and by using the Scherrer equation, the particle size was calculated. UV–Visible diffuse reflectance spectroscopy reveals the characteristic absorbance peak at 373 nm and gives the band gap nearly 3.23 eV for synthesized (ZnO NPs) due to the quantum confinement effect. Transmission electron microscopy (TEM) shows spherical-shaped particles. The products (ZnO-NPs) have a good effect on antibacterial activity against different types of bacteria. After 7 hours, the degradation rate of methylene blue (MB) dye by synthesized ZnO-NPs as a photocatalyst is 92.28 % from ZnO NPs synthesized at 30 oC.

Keywords: Green synthesis, ZnO nanoparticles, photocatalyst, Methylene blue (MB), Ocimum Basilicum extract.

.

1. Introduction

Nanotechnology is a field that treaty with materials on Nanoscale level, where it studies the matters in size of (1_100) nm, The decreasing of materials size gives a lot of new physical and chemical properties, so there are large applications for these materials in different fields such as material science, industry, and biomedical fields [1], [2].

The methods of synthesis nanoparticles are several, where the easiest and most effective way is green synthesis, also known as biosynthesis, which is an eco-friendly and non-toxic method, it can use organisms and plant or plant extracts to act as capping and reducing agents [3]. There are many advantages of biosynthesized nanoparticles, especially the application for biomedical purposes or environmental systems, this is due to the reduction or low level of toxicity, the energy and costs associated with these nanoparticles compared to those prepared through physical and chemical methods, so we can use them in many applications [1], [4], [5].

Water pollution is one of the main reasons for gradually increasing environmental pollution. Therefore, there is a strong need for safe and cost-effective water purification methods. Photocatalytic degradation based on heterogeneous semiconductors is one of the safest, simplest, and most cost-effective methods for removing dyes and organic compounds from polluted water from industries and residences[2], [6].

Zinc oxide nanoparticles (ZnO-NPs) have attracted exciting research importance due to their huge horizon of applications such as photocatalytic degradation, targeted drug delivery, antioxidant activity, antibacterial activity, biosensors, and eco-friendly remediation [5]–[7]. Of these, ZnO NPs are of the most important because they are low-cost to produce, safe, and can be prepared easily. ZnO NPs exhibit great semiconducting properties because

*Corresponding author: *e-mail: Mahmoud.abdelsadek@sci.svu.edu.eg

DOI : 10.21608/EJPHYSICS.2022.157467.1084

Received: 20/8/2022; accepted: 29/9/2022

of their large bandgaps (3.37 eV), such as high catalytic activity, optics, and UV filtering properties. It can be used to remove Sulphur and arsenic from water [7], [8].

The current study focuses on plant-mediated green synthesis of ZnO NPs via Ocimum Basilicum extracts at different temperatures and uses them in environmental applications (wastewater treatment and antibacterial activity).

2. Experimental

a.Materials and extract preparation:

All the chemicals were utilized as received without further purification they include zinc acetate dihydrate ($C_4H_6O_4Zn.2H_2O$_98%) (Sigma-Aldrich_mark) was used as a precursor salt, sodium hydroxide pellets (NaOH_98%) (Oxford_mark), $NaBH_4$ (SdS_mark) and methylene blue (MB).The extract of *Ocimum Basilicum* is used as a reducing and capping agent was prepared from *Ocimum Basilicum leaves* collected from the South Valley University (SVU) campus, Qena. The fresh leaves of *Ocimum Basilicum* were washed with tap water to remove dust particles, then dried in the open air and pulverized using a blender. In a 250 mL conical flask, 6 g of powdered leaves were soaked in 100 mL of deionized water, shaken for 2h and then filtered through a tissue (cloth), then centrifugated for 5 min at 15000 rpm, and the plant extract was put in an air-tight bottle and stored in the refrigerator at 4 ºC.

b.Green synthesis of zinc oxide NPs

ZnO nanoparticles were prepared with some modifications according to [5], [9]. The modifications are found in the extract kind, the concentration of metal salt, and the extract and reaction time. For the preparation of ZnO NPs, the green route was used. The vessel containing an aqueous solution of 25 ml of extract from *Ocimum Basilicum* (6%) was under continuous stirring. A solution of zinc acetate dihydrate ($C_4H_6O_4Zn.2H_2O$) (20 ml, 1 M) was added dropwise to this solution under continuous stirring. The sample's ph was then raised to 11 by adding NaOH (1 M) solution dropwise, resulting in an off-white solution. Finally, the mixture was heated to 30 ^oC, 60 ^oC, and 90 ^oC for 1 hour. When the temperature was higher, the colour became white, and we left the mixture for the next day for aging. After that, the solution was centrifuged and washed with distilled water many times and alcohol and dried at 35°C then calcined at 500°C for 2 hours. Hereafter, the prepared samples will be termed as A1, A2, and A3 for samples synthesized at 30 °C, 60 °C, and 90 °C respectively.

3. Characterization

The crystal structures of pure ZnO, pure MgO, and $Zn_{1-x}Mg_xO$ nanocomposites were analyzed by (Philips, PW 1710) X-ray diffractometer with CuKα line (λ = 1.54183Å) in the range 2θ from 10° to 90°. The data derived from investigating XRD peaks of ZnO NPs were carried out to calculate the crystallite size and the lattice strain based on both Scherrer formula and Williamson–Hall model. The functional groups of tested samples were recorded by FTIR spectrum (JASCO FT-IR 4100) in the range of wavenumber between 4000 and 400 cm^{-1}. The morphology of the synthesized samples was carried out by a High-Resolution transmission Electron Microscope of type (Philips, EM-2100 PW 1710 Japan). JASCO 670 UV spectrophotometer was used to measure the UV–Vis'sabsorption spectrum of the samples in the range from 200 to 800 nm. A photoluminescence study was performed using a fluorescence spectrophotometer (JASCO 860j0) under an excitation wavelength of 320 nm.

a. Photocatalytic activity

The photocatalytic activities of the ZnO nanoparticles were studied by the degradation of Methylene blue (MB) under UV-visible irradiation. In this experiment, 0.1 g of ZnO catalyst was added into 100 ml of 10 ppm of MB solution in a reaction vessel, then 20 ml of sodium borohydride (NaBH4_10 mM) solution as a reduction agent. After that, the mixture was exposed to ultraviolet light (TUV 8W G8T5, λ= 254 nm) with continuous stirring. At regular intervals, aliquots (5 ml) of the reaction solution were centrifuged to separate the powders and analyzed by a UV–visible spectrophotometer. Where the degradation rate can be calculated using the following equation:

$$degradation\ rate\ \% = (A_0 - A_t) * 100 \quad (1)$$

where, A_0 = the absorbance value at t =0, and A_t = absorbance at time (t) [10]. The following equations can be used to determine a kinetics of photocatalyst degradation of MB dye in the presence of ZnO NPs:

$$\ln\frac{A_0}{A_t} = kt \quad (2)$$

..
where k is first order rate constant (min^{-1}) [11].

b.Antibacterial activity

The inhibitory effect of ZnO NPs on food pathogenic bacteria was tested using the disc diffusion method. To test the inhibitory effect of ZnO nanoparticles, four strains were used in the present study; two of Gram-positive bacteria (*Bacillus cereus* DSMZ 345, *Staphylococcus aureus* ATCC 29213) and two of Gram-negative bacteria (*Escherichia coli* O157:H7 ATCC 43895, and *Salmonella enterica serovar Typhimurium* ATCC 23564. The strains were obtained from the Cairo Microbiological Resources Centre (Cairo-MIRCEN), Egypt. Working stock cultures were kept at −70 °C in 15% v/v glycerol/brain–heart infusion (BHI) broth. For routine work, strains were cultivated on BHI agar and stored at 4 °C on slants. Five samples of different concentrations of the zinc oxide solutions were used: 10, 20, 30, 40, and 50 µg /ml.

4. Results and Discussion

4.1. Thermal analysis

Thermal analysis spectra of $Zn_{1-x}Mg_xO$ nanocomposite

Studying the Thermal Gravimetric (TG) and Differential Scanning Calorimetry (DSC) curves is displayed in Fig. 1 for ZnO NPs at 60 ^oC as an example. In Fig. 1, the TG curve shows that, at 180 °C the weight loss reaches (25.5 %) due to the removal of water from the surface of the sample, and from 200 to 450 °C there is a slight weight loss, which can be attributed to the removal of the organic compound. The synthesized ZnO-NPs after that became more thermally stable, so 500 °C was chosen as the suitable temperature for calcination [12], [13]. The total weight loss from the sample was nearly 29.6%. In the DSC curve, the endothermic peak appears at 146.7 °C due to the evaporation of water molecules on the surface of the ZnO-NPs [14].

.

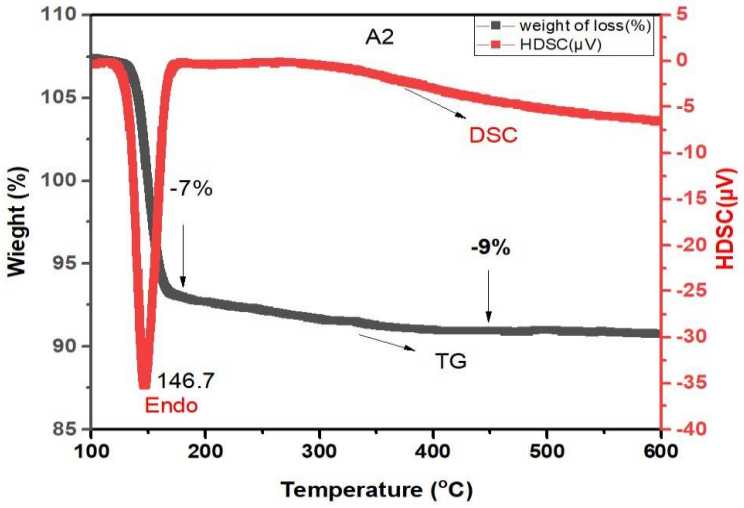

Fig. 1. TG and DSC curves of synthesized ZnO NPs (A2).

4.2. Structure and morphological analysis

4.2.1. XRD Analysis

The XRD pattern of the green synthesized ZnO nanoparticles is shown in Fig. 2, which indicates the single–phase hexagonal structure of ZnO with lattice constants (a = 3.24170 and c = 5.18760 Å) [5], [8]. In the pattern, there is no impurity peak, which shows a complete decrease of the precursor into NPs and pure crystalline ZnO NPs [6]. Also, from Fig. 2, with increasing temperature, the crystallinity increased [5].From Scherrer's equation, the average crystallite size of synthesized ZnO could be determined as:

$$D = \frac{k\lambda}{\beta \cos\theta} \qquad (3)$$

where D is the average crystal size (nm), k is a constant equal to 0.94, λ is the Cu-Kα radiation wavelength (1.54060 Å), □ is the full-width at half maximum (FWHM) of the peak (in radians), and θ is the Bragg angle (degree) [15], [16]. The average crystal size for A1, A2, and A3 was (25.573319, 25.012259, and 24.8009) nm, respectively, which decreased with temperature.

The crystal size is used to estimate the number of defects and vacancies in the crystal, which is known as the dislocation density and can be calculated using the following equation [17]:

$$\delta = \frac{1}{D^2} \qquad (4)$$

where δ is the dislocation density and D is the average crystallite size.In general, we conclude that as temperature rises, particle size decreases because the conversion of Zn^{2+} ions into $Zn(OH)^2$ occurs more quickly due to thermally agitated OH ions, leaving no free ions to aggregate and decrease particle size [18].

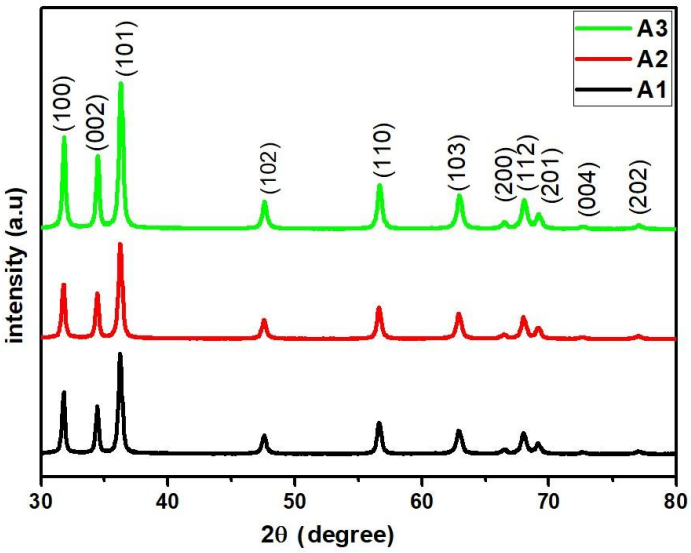

Fig. 2. XRD patterns of ZnO nanoparticles were prepared at different temperatures (A1, A2, and A3).

4.2.2. Morphological analysis and EDX spectra

TEM micrographs were thought to be a better instrument for evaluating size and morphology since they provide actual pictures from which measurements could be obtained [19]. Figure 3 gives information about size and morphology of synthesized ZnO nanoparticles (A1, A2, and A3) where indicated that spherical shape particles.

The EDX (energy-dispersive X-ray spectroscopy) show the presence of Zinc and Oxygen elements and no contaminants were identified under the EDX detection limit [20], which is seen in Fig. 4.

..

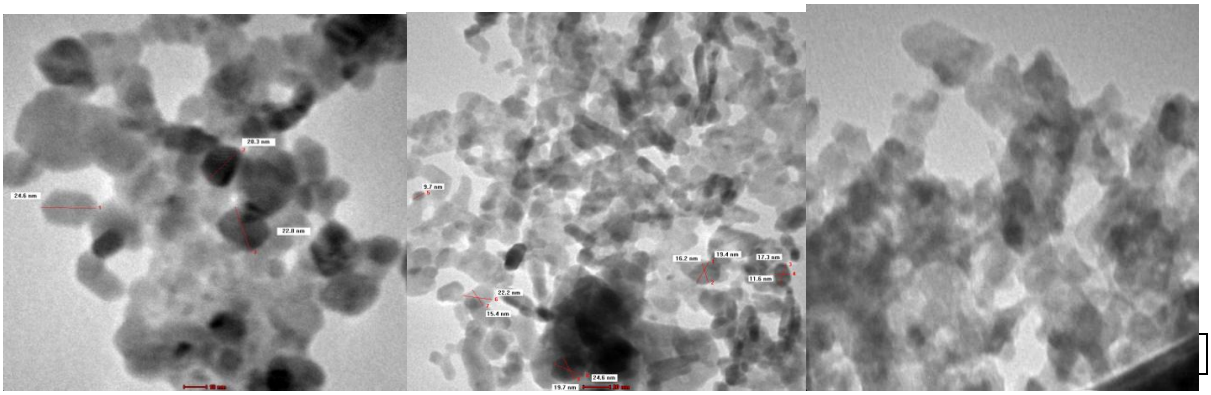

Fig. 3. TEM images for ZnO nanoparticles (A1, A2, and A3), respectively.

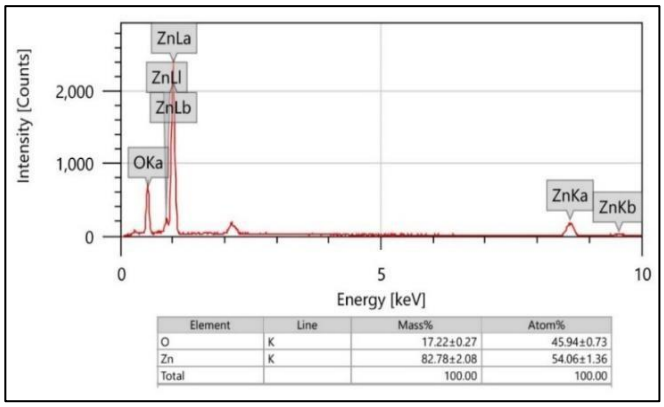

Fig. 4. EDX of ZnO NPs (A2)

4.3.FTIR spectra

The functional groups existing on synthesized ZnO NPs can be identified by Fouriertrans form infrared spectroscopy (FT-IR spectroscopy), which is categorized in the range 400– 4000 cm^{-1}, where is plotted as shown in Fig, 5. Figure 5 indicates that the main absorption bands at 3418 cm^{-1} represent the O–H stretching vibration of water, The peaks observed at 2337 cm^{-1} represent the vibrations representing C-H that are adsorbed from alkenes [14]. The peaks recorded around 1518 cm^{-1} are probably from the bending vibration of the C=O bond [14], [21]. The peaks around 1065 cm^{-1} represent the stretching vibration of C–O attributed to zinc acetate [17].The band centered at 1070 cm^{-1} is attributed to the C-O-C [22]. The band at 870 cm^{-1} refers to C-H. The Zn–O complex is represented by the band between 400 and 560 cm^{-1} [6], [23]. The figure confirmed the synthesis of zinc oxide by using the green method.

4.4. Optical properties

The optical properties of ZnO nanoparticles synthesized by the green method are calculated by using UV–Visible diffuse reflectance spectroscopy in the range of 200–800 nm, as shown in Fig 6. The absorbance peaks are nearly identical to each other, which is also clear in the result of the crystal size. All prepared samples cleared absorbance peaks at nearly 373 nm. Where the figure shows all the absorption peaks of the samples less than that of bulk ZnO (388 nm) [17], this is attributed to a reduction in particle size [18]. Figure 7 indicated that the diffused reflectance spectra for the samples exhibited a significant rise at 380 nm and had high reflecting characteristics beyond around 437 nm. This was owing to the increased probability of photons lacking the necessary energy to interact with electrons or atoms reflecting [14]. We can use the result of UV–Visible spectroscopy to determine the optical bandgap of samples. Where it is estimated using Tauc's equation:

$$(\alpha h\nu)^{2} = A(h\nu - E_g) \qquad (5)$$

Where A is a constant, hν is the energy of the photon, α is the absorption coefficient, and Eg is the energy bandgap. For calculating the band gap, the draw relationships between $(\alpha h\nu)2on$ the y-axis and $(h\nu)$ on the x-axis is as shown in Fig. 8, where the bandgap is determined by extrapolating the linear portion of the graph on the x-axis [17], [18]. So, the bandgap of samples is (3.216, 3.226, 3.220 eV) for (A1, A2, and A3), respectively. From the bandgap values, it is indicated that there is a decrease in values from about the bulk value of ZnO NPs (3.37 eV). In Table 1, the relatively small increases in a and c in the cell parameters may be attributed to the evident decrease in ZnO NS band gap values from bulk (3.37 eV). As a result, any change in the lattice parameters results in a change in the electronic band gap [24].

For the results, it showed that the difference in extract kinds and the concentrations of extract and metal salt from the last study [5], [25],led to disagreeing in the behaviour of the particle size and the optical properties. This work indicated, XRD results show that the particle size decreases with temperature and there is high absorbance peak at 30 oC.

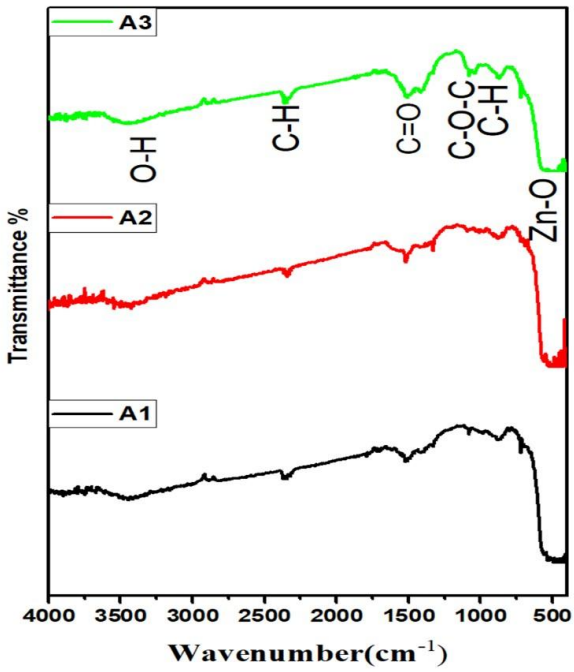

Fig. 5. FTIR spectrum of ZnO nanoparticles green synthesized (A1, A2, and A3).

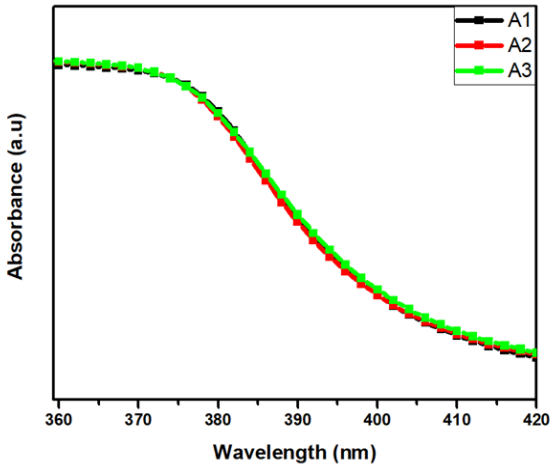

Fig. 6. UV–Visible absorbance spectroscopy ZnO nanoparticles (A1, A2, and A3)

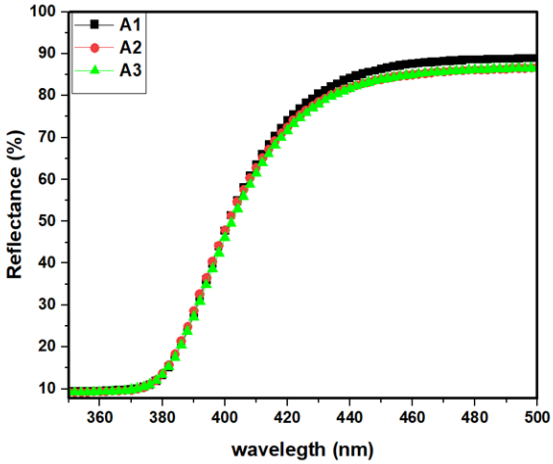

Fig. 7. UV–visible diffuse reflectance of ZnO of nanoparticles (A1, A2, and A3)

..

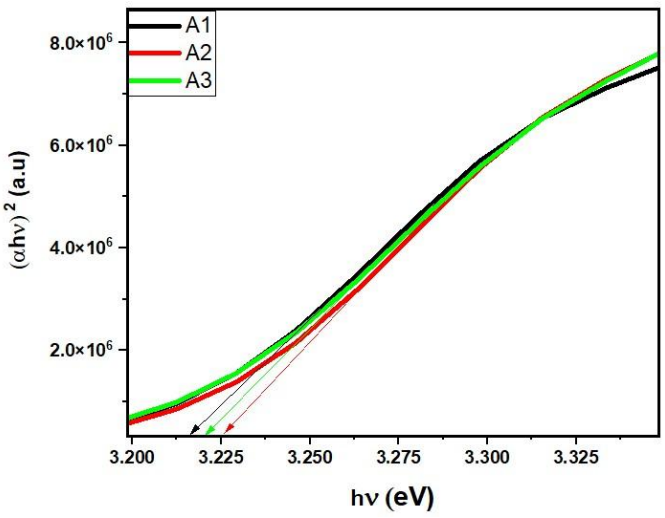

Fig. 8. Energy gap of the ZnO nanoparticles synthesized (A1, A2, and A3).

TABLE 1. The result of obtained by Scherrer's equation and Dislocation density (δ) and Strain (ε).

Sample	Temperature (□ C)	Scherrer (D) (nm)	Dislocation density (□)(nm^{-2})	a (Å)	c (Å)	E_g (eV)
A1	30 □C	25.57	1.529×10^{-3}	3.24	5.19	3.22
A2	60 □C	25.01	1.598×10^{-3}	3.24	5.19	3.23
A3	90 □C	24.80	1.626×10^{-3}	3.25	5.21	3.22

4.5. Photocatalytic activity of ZnO NPs

Under UV light irradiation (lamb), the photocatalytic activity of green-produced ZnO NPs is tested in degrading MB dye. The degradation rate of MB dye was estimated by equation (1). Figure 9 gives the UV-visible spectra of the degradation rate for MB at the diverse time (1– 7h) for synthesized ZnO NPs with different temperatures. It indicated that with an increase in the irradiation time, the colour of MB would be decreased. Where the decrease in the MB peaks (662 nm) refers to the concentration of the dye. At 1 h, without ZnO NPs, the degradation rate was 18%, but when the nanoparticles (0.1 g) were added, the degradation rate reached 59.58%. It is clear that the NPs have a good effect on the dye. Table 2 refers to the degradation rate of synthesized ZnO NPs at different temperatures. Table 2 shows that A1 is the best one where degradation for the MB reaches 92.28%, at 7 h. A first order rate constant (k) value was determined from the plot of ln (At/Ao) vs. irradiation time (t) (Fig. 10) to study the effect of UV irradiation time on the degradation process and was found to be 0.2239 min-1 and R2 = 0.935, which refers to the fitted line's correlation coefficient [26]. Figure 11 indicates the bar graph of the degradation rate of MB dye for samples (A1-A3) with respect to irradiation time (1 and 7h).

Mechanism of Photocatalytic activity Methyl Blue (MB): Figure 12 shows themechanism of photocatalytic activity of Methyl Blue (MB) by synthesized ZnO NPs. Photoelectron (e-CB) and photo-induced holes (h+VB) are generated when a photon (light) reacts with ZnO nanoparticles. To oxidize organic dyes like MB, photoelectrons are held by adsorbed O2 as electron acceptors, while photo-induced holes are absorbed by negative species like OH- or organic pollutants. The photocatalytic reaction mechanism for this is as follows:

$$ZnO + h\nu \rightarrow ZnO\,(h_{VB+} + e_{CB-}) \quad (5)$$

$$h_{VB} + + OH^- \rightarrow OH^{\bullet} \quad (6)$$

$$e_{cB} - + O_2 \rightarrow O^{2\bullet -} \quad (7)$$

$$O^{2\bullet -} + organic\ pollutants \rightarrow Oxidation\ products \quad (8)$$

$$OH^{\bullet} + organic\ pollutants \rightarrow Oxidation\ products \quad (9)$$

The degradation of organic contaminants in wastewater into less hazardous minerals like CO2 and H2O is aided by active oxygen species (O2•, O-2) and hydroxyl free radicals (•OH, OOH•).

According to these studies, photocatalyst ZnO NPs are extremely suited for environmental purification procedures [27]–[29]

These results show that ZnO NPs synthesized by a green method, using the extract of Ocimum Basilicum, are not only excellent for use in the degradation of contaminants in water, but they are also proving the harmfulness of green synthesized ZnO NPs against the bacterial strains studied it investigations reported in the literature (see Table 3).

..

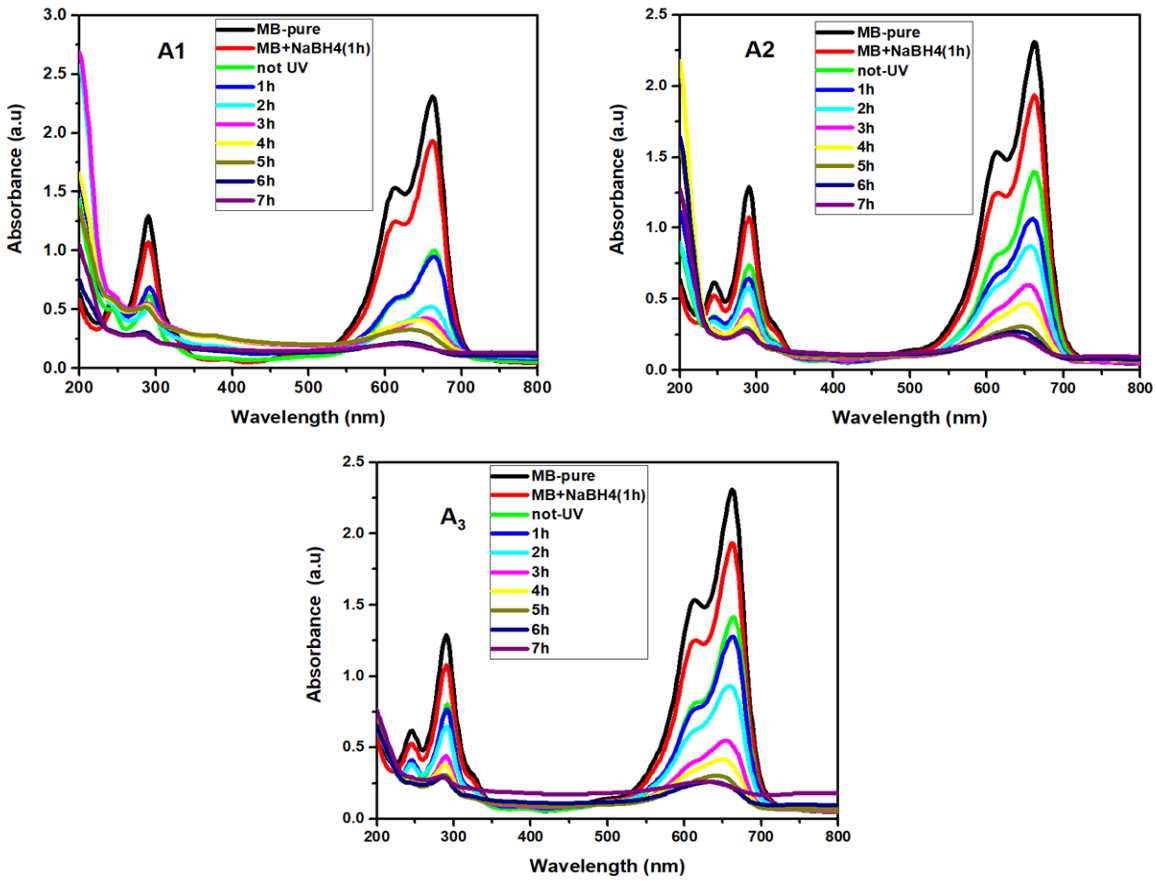

Fig. 9. Photocatalyst activity of produced ZnO NPs (A1, A2 and A3).

TABLE 2. Degradation rate of synthesized ZnO NPs (0.1g) (A1, A2 and A3).

Sample	Time (hour)	Degradation rate (%)
A1	1	59.58
A1	7	92.28
A2	1	53.56
A2	7	92.11
A3	1	48.4
A3	7	90.59
The mixture without ZnO NPs	1	16.49

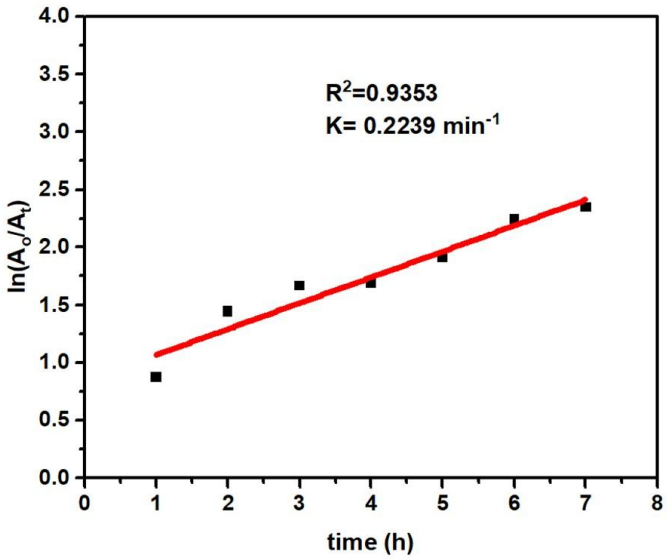

Fig. 10. Kinetic study for A1.

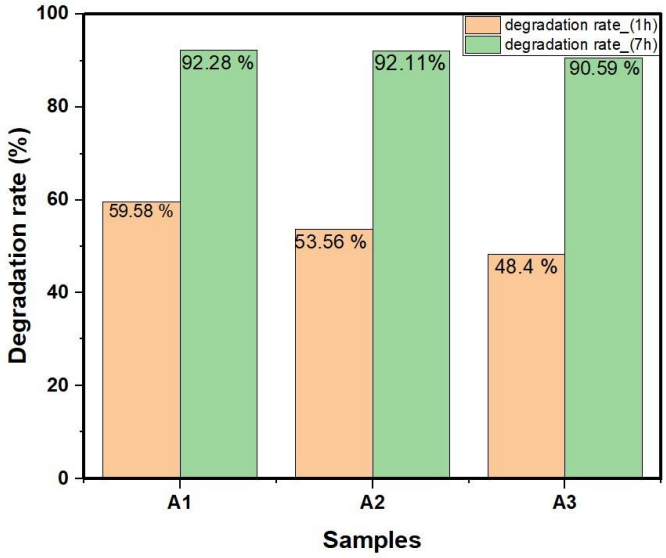

Fig. 11. Bar graph of degradation rate of MB dye for samples (A1, A2 and A3) with respect to irradiation time (1 and 7h).

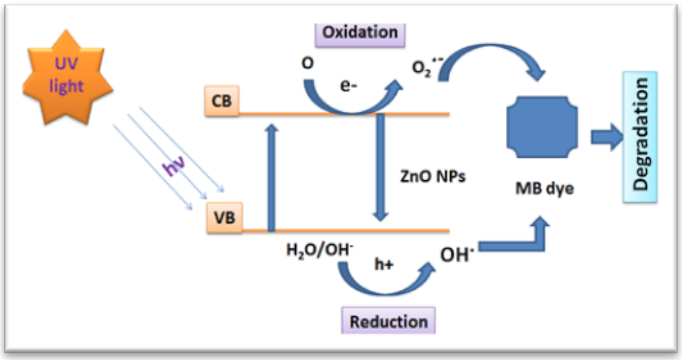

Fig. 12. Mechanism of degradation of MB dye by synthesized ZnO NPs.

..

TABLE 3. Green synthesis studies of ZnO NPs and their application in photocatalytic activity.

year	NPs	Extract	Catalyst (g)	NPs size (nm)	Pollutant	Degradation time (min)	Reference
2017	ZnO	Eucalyptus globulus	0.025	11.6	MB	50 (98.3% degradation)	[27]
2018	ZnO	E. tirucalli plant	0.020	20	MB	120 (40% degradation)	[28]
2020	ZnO	Azadirachta Indica (Neem)	5	25.97	MB	200 (80% degradation)	[30]
2021	ZnO	SyzygiumCumini	0.2	10-12.5	MB	180 (91.40% degradation)	[31]
2022	ZnO	*Ocimum Basilicum*	0.01	25	Rh-B	100 (91.4% degradation)	[32]
2022	ZnO	*Ocimum Basilicum*	0.1	25.57	MB	420 (92.28% degradation)	This work

4.6. Antibacterial activity

The effect of the ZnO NPs on different gram-positive and gram-negative bacteria with different doses (10, 20, 30, 40 and 50 µg /ml) was shown in Table 4. Figure 13, for example, shows the inhibition zones for Staphylococcus aureus (ATCC 29213) at various doses of ZnO NPs (A1, A3). From Table 4, with the increasing concentration of the ZnO NPs, the inhibition zones will increase.

In the present study, gram-positive bacteria (Staphylococcus aureus ATCC 29213, Bacillus cereus DSMZ) showed a higher response to the ZnO nanoparticles as compared to gram-negative bacteria (Escherichia coli O157:H7 ATCC, Salmonella enterica serovar Typhimurium ATCC 23564). In addition, S. aureus ATCC 29213, B. cereus DSMZ showed the highest (31 and 26 mm respectively) and E. coli O157:H7 ATCC, and S. enterica serovar Typhimurium ATCC 23564 showed the lowest (18 and 9 mm respectively) zones of inhibition at a dilution of 50 g/µl, which is clear in Table 4. Furthermore, the antibacterial activity of ZnO samples A2 and A3 was much stronger than that of ZnO sample A1. This could be simply explained as smaller particles A2 and A3 normally have a larger surface-to-volume ratio, which provides a more efficient means for antibacterial activity. The result is reported to show that there is efficient antibacterial activity for biosynthesis. ZnO NPs have a large surface area, which gives good contact between microorganisms and nanoparticles, so it is clear that there exists an inverse relationship between antibacterial activity and nanoparticle size[33]. The study shows that the inhibition zone can be increased by increasing the concentration of ZnO nanoparticles in the discs. These results achieve better results than other investigations reported in the literature [22], [29], [34] [35].

Mechanism of Antibacterial activity: Reactive oxygen species such as H2O2, hydroxyl radicals, singlet oxygen, and Zn+2 ions produced on the surface of ZnO, which may permeate the cell, are responsible for the antibacterial action [36]. Figure 14 indicates the bar graph of the inhibition zone for different ZnO NPs samples (A1-A3) against positive and negative gram.

TABLE 4. Antibacterial activity of ZnO NPs clears against negative and positive type of bacterial.

Samples µg/ml		Inhibition zone (mm)				Ceftriaxone CRO 30 mcg
		Staphylococcusaureus ATCC 29213 **(Gram +Ve)**	*Bacilluscereus* DSMZ **(Gram +Ve)**	*Escherichiacoli* O157:H7ATCC **(Gram -Ve)**	*Salmonellaentericas*erovar ATCC 23564 **(Gram -Ve)**	
A1	10	17	19	8	0	0
	20	27	20	9	6	
	30	23	23	10	6	
	40	25	24	12	8	
	50	27	28	14	11	
A2	10	23	10	12	0	0
	20	25	20	13	0	
	30	27	22	13	9	
	40	30	26	15	9	
	50	31	26	18	9	
A3	10	22	12	13	12	0
	20	25	16	16	13	
	30	25	22	17	17	
	40	29	25	18	17	
	50	29	27	19	19	

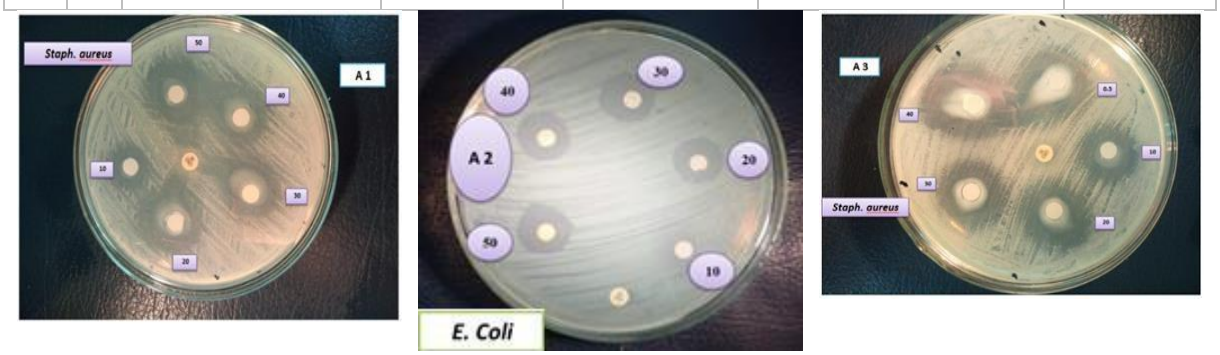

Fig. 13. Inhibition Zone for Different Samples of ZnONPs (A1 and A3) samples to *Staphylococcus aureus* ATCC 29213) and *Escherichia coli* O157:H7 ATCC of A_2.

..

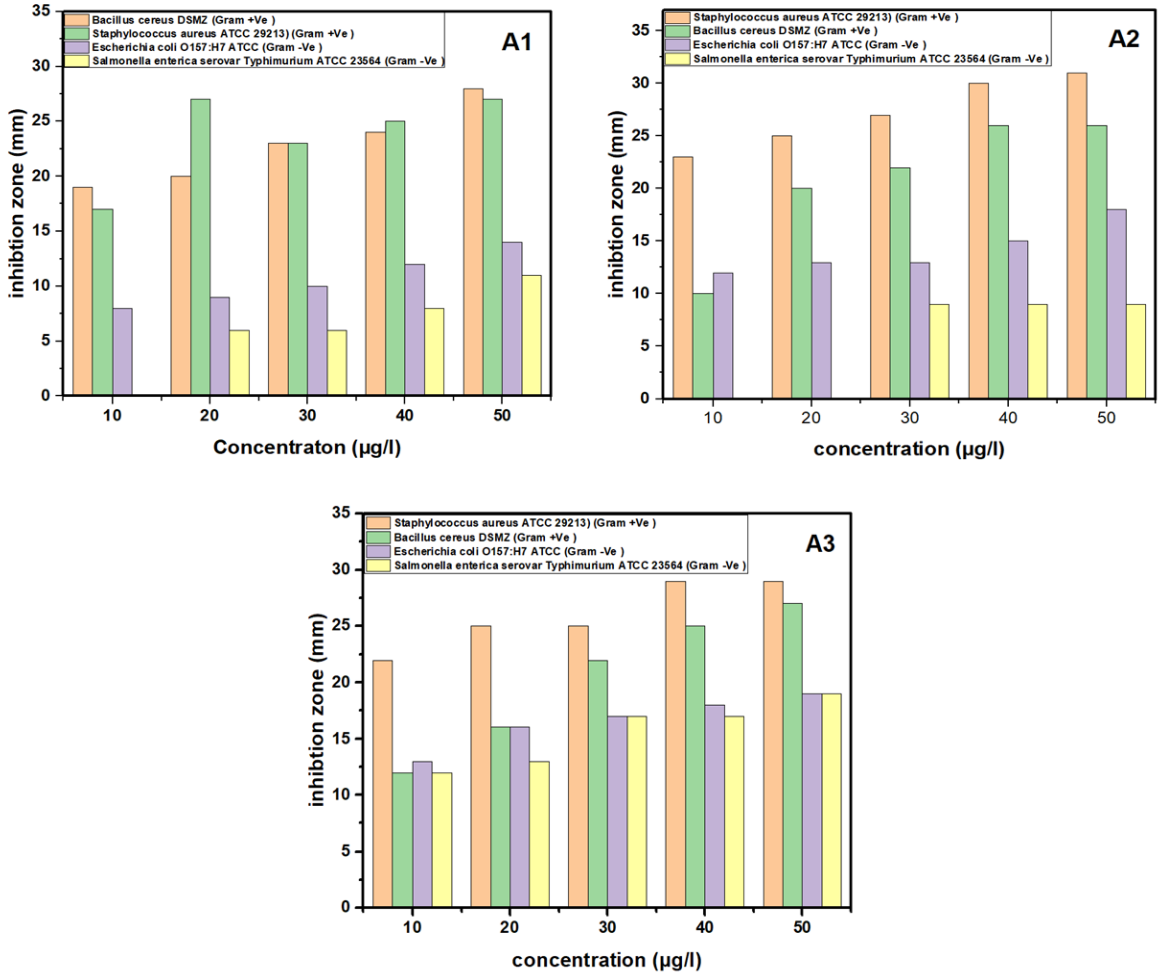

Fig. 14. Bar Graph of Inhibition Zone for Different ZnO Nanoparticles Samples (A1, A2 and A3) against positive and negative gram.

Conclusions

The present work ZnO NPs with different temperatures have been successfully prepared by green synthesis using extract of Ocimum Basilicum as a reducing and stabilizing agent. To study the samples, several equipment's were used to characterize ZnO NPs samples, such as thermal analysis, UV–Visible diffuse reflectance spectroscopy, FTIR spectra, XRD analysis, TEM analysis, and EDX spectra. All ZnO samples were found in the crystalline hexagonal wurtzite phase and their crystallite size lie in nano-sized structure between 25.01 and 24.8 nm. ZnO NPS exhibit band gap between 3.22 and 3.23 eV below the standard value (3.37 eV) due to changes in lattice parameters. Finally, the produced sample would be used in two applications: photocatalysis and antibacterial activity. It has good behaviour against MB, and positive and negative gram.

Acknowledgement

The authors would like to thank the Faculty of Science, South Valley University, Qena-83523 Egypt.

References

[1] A. M. Pillai *et al.*, “Green synthesis and characterization of zinc oxide nanoparticles with antibacterial and antifungal activity,” *J. Mol. Struct.*, vol. **1211**, p. 128107, 2020, doi: 10.1016/j.molstruc.2020.128107.

[2] B. Praveen kumar, M. Arthanareeswari, S. Devikala, M. Sridharan, J. Arockia selvi, and T. Pushpa malini, “Green

synthesis of zinc oxide nanoparticles using typha latifolia. L leaf extract for photocatalytic applications," *Mater. Today Proc.*, vol. **14**, pp. 332–337, 2019, doi: 10.1016/j.matpr.2019.04.155.

[3] N. Nagar and V. Devra, "Green synthesis and characterization of copper nanoparticles using Azadirachta indica leaves," *Mater. Chem. Phys.*, vol. **213**, pp. 44–51, 2018, doi: 10.1016/j.matchemphys.2018.04.007.

[4] F. M. Mohammadi and N. Ghasemi, "Influence of temperature and concentration on biosynthesis and characterization of zinc oxide nanoparticles using cherry extract," *J. Nanostructure Chem.*, vol. **8**, no. 1, pp. 93–102, 2018, doi: 10.1007/s40097-018-0257-6.

[5] N. Bala *et al.*, "Green synthesis of zinc oxide nanoparticles using Hibiscus subdariffa leaf extract: Effect of temperature on synthesis, anti-bacterial activity and anti-diabetic activity," *RSC Adv.*, vol. **5**, no. 7, pp. 4993–5003, 2015, doi: 10.1039/c4ra12784f.

[6] M. Rafique *et al.*, "Plant-mediated green synthesis of zinc oxide nanoparticles from Syzygium Cumini for seed germination and wastewater puri," *Int. J. Environ. Anal. Chem.*, vol. 00, no. 00, pp. 1–16, 2020, doi: 10.1080/03067319.2020.1715379.

[7] H. Agarwal, S. Venkat Kumar, and S. Rajeshkumar, "A review on green synthesis of zinc oxide nanoparticles – An eco-friendly approach," *Resour. Technol.*, vol. **3**, no. 4, pp. 406–413, 2017, doi: 10.1016/j.reffit.2017.03.002.

[8] Y. A. Selim, M. A. Azb, I. Ragab, and M. H. M. Abd El-Azim, "Green Synthesis of Zinc Oxide Nanoparticles Using Aqueous Extract of Deverra tortuosa and their Cytotoxic Activities," *Sci. Rep.*, vol. **10**, no. 1, pp. 1–9, 2020, doi: 10.1038/s41598-020-60541-1.

[9] A. S. Abdelsattar, W. M. Farouk, S. Mohamed, and A. Safwat, "Utilization of Ocimum basilicum extracts for zinc oxide nanoparticles synthesis and their antibacterial activity after a novel combination with phage," *Mater. Lett.*, vol. **309**, no. October 2021, p. 131344, 2022, doi: 10.1016/j.matlet.2021.131344.

[10] P. Fageria, S. Gangopadhyay, and S. Pande, "Synthesis of ZnO/Au and ZnO/Ag nanoparticles and their photocatalytic application using UV and visible light," *RSC Adv.*, vol. **4**, no. 48, pp. 24962–24972, 2014, doi: 10.1039/c4ra03158j.

[11] A. A. Alshehri and M. A. Malik, "Facile one-pot biogenic synthesis of cu-co-ni trimetallic nanoparticles for enhanced photocatalytic dye degradation," *Catalysts*, vol. **10**, no. 10, pp. 1–21, 2020, doi: 10.3390/catal10101138.

[12] N. T. Nguyen and V. A. Nguyen, "Synthesis, Characterization, and Photocatalytic Activity of ZnO Nanomaterials Prepared by a Green, Nonchemical Route," *J. Nanomater.*, vol. 2020, 2020, doi: 10.1155/2020/1768371.

[13] O. R. Vasile *et al.*, "Influence of the size and the morphology of ZnO nanoparticles on cell viability," *Comptes Rendus Chim.*, vol. **18**, no. 12, pp. 1335–1343, 2015, doi: 10.1016/j.crci.2015.08.005.

[14] A. A. Alshehri and M. A. Malik, "Biogenic fabrication of ZnO nanoparticles using Trigonella foenum-graecum (Fenugreek) for proficient photocatalytic degradation of methylene blue under UV irradiation," *J. Mater. Sci. Mater. Electron.*, vol. **30**, no. 17, pp. 16156–16173, 2019, doi: 10.1007/s10854-019-01985-8.

[15] A. A. Essawy, I. H. Alsohaimi, M. S. Alhumaimess, H. M. A. Hassan, and M. M. Kamel, "Green synthesis of spongy Nano-ZnO productive of hydroxyl radicals for unconventional solar-driven photocatalytic remediation of antibiotic enriched wastewater," *J. Environ. Manage.*, vol. **271**, no. May, p. 110961, 2020, doi: 10.1016/j.jenvman.2020.110961.

[16] K. P. Raj and K. Sadayandi, "Effect of temperature on structural, optical and photoluminescence studies on ZnO nanoparticles synthesized by the standard co-precipitation method," *Phys. B Condens. Matter*, vol. **487**, pp. 1–7, 2016, doi: 10.1016/j.physb.2016.01.020.

[17] M. J. Chithra, M. Sathya, and K. Pushpanathan, "Effect of pH on crystal size and photoluminescence property of zno nanoparticles prepared by chemical precipitation method," *Acta Metall. Sin. (English Lett.*, vol. **28**, no. 3, pp. 394–404, 2015, doi: 10.1007/s40195-015-0218-8.

[18] V. Koutu, L. Shastri, and M. M. Malik, "Effect of temperature gradient on zinc oxide nano particles synthesized at low reaction temperatures," *Mater. Res. Express*, vol. **4**, no. 3, 2017, doi: 10.1088/2053-1591/aa5855.

[19] R. Yogamalar, R. Srinivasan, A. Vinu, K. Ariga, and A. C. Bose, "X-ray peak broadening analysis in ZnO nanoparticles," *Solid State Commun.*, vol. **149**, no. 43–44, pp. 1919–1923, 2009, doi: 10.1016/j.ssc.2009.07.043.

[20] G. S, A. Belay, C. Reddy AR, and B. Z, "Synthesis and Characterizations of Zinc Oxide Nanoparticles for

..
Antibacterial Applications," *J. Nanomed. Nanotechnol.*, vol. **s8**, no. May, 2017, doi: 10.4172/2157-7439.s8-004.

[21] M. S. Abd El-sadek, H. S. Wasly, and H. S. El-Sheshtawy, "CdS@Mn(OH)2 nanocomposites: Novel aqueous synthesis, structural and optical properties," *Eur. Phys. J. Plus*, vol. **133**, no. 12, pp. 2–8, 2018, doi: 10.1140/epjp/i2018-12403-5.

[22] S. Tantiwatcharothai and J. Prachayawarakorn, "Characterization of an antibacterial wound dressing from basil seed (Ocimum basilicum L.) mucilage-ZnO nanocomposite," *Int. J. Biol. Macromol.*, vol. **135**, pp. 133–140, 2019, doi: 10.1016/j.ijbiomac.2019.05.118.

[23] T. V. Surendra, S. M. Roopan, N. A. Al-Dhabi, M. V. Arasu, G. Sarkar, and K. Suthindhiran, "Vegetable Peel Waste for the Production of ZnO Nanoparticles and its Toxicological Efficiency, Antifungal, Hemolytic, and Antibacterial Activities," *Nanoscale Res. Lett.*, vol. **11**, no. 1, 2016, doi: 10.1186/s11671-016-1750-9.

[24] M. R. Parra and F. Z. Haque, "Aqueous chemical route synthesis and the effect of calcination temperature on the structural and optical properties of ZnO nanoparticles," *J. Mater. Res. Technol.*, vol. **3**, no. 4, pp. 363–369, 2014, doi: 10.1016/j.jmrt.2014.07.001.

[25] F. Malek and M. Nahid, "Influence of temperature and concentration on biosynthesis and characterization of zinc oxide nanoparticles using cherry extract," *J. Nanostructure Chem.*, vol. **8**, no. 1, pp. 93–102, 2018, doi: 10.1007/s40097-018-0257-6.

[26] N. A. S. Ridha, H. K. Egzar, and N. M. Kamal, "Synthesis and characterization of CuO nanoparticles and TiO2/CuO nanocomposite and using them as photocatalysts," *AIP Conf. Proc.*, vol. **2290**, no. December, 2020, doi: 10.1063/5.0029408.

[27] S. Balaji and M. B. Kumar, "Facile green synthesis of zinc oxide nanoparticles by Eucalyptus globulus and their photocatalytic and antioxidant activity," *Adv. Powder Technol.*, vol. **28**, no. 3, pp. 785–797, 2017, doi: 10.1016/j.apt.2016.11.026.

[28] K. H. Sudheer Kumar, N. Dhananjaya, and L. S. R. Yadav, "E. tirucalli plant latex mediated green combustion synthesis of ZnO nanoparticles: Structure, photoluminescence and photo-catalytic activities," *J. Sci. Adv. Mater. Devices*, vol. **3**, no. 3, pp. 303–309, 2018, doi: 10.1016/j.jsamd.2018.07.005.

[29] T. S. Aldeen, H. E. Ahmed Mohamed, and M. Maaza, "ZnO nanoparticles prepared via a green synthesis approach: Physical properties, photocatalytic and antibacterial activity," *J. Phys. Chem. Solids*, vol. **160**, no. August 2021, p. 110313, 2022, doi: 10.1016/j.jpcs.2021.110313.

[30] M. J. Haque, M. M. Bellah, M. R. Hassan, and S. Rahman, "Synthesis of ZnO nanoparticles by two different methods & comparison of their structural, antibacterial, photocatalytic and optical properties," *Nano Express*, vol. **1**, no. 1, p. 010007, 2020, doi: 10.1088/2632-959x/ab7a43.

[31] H. Sadiq *et al.*, "Green synthesis of ZnO nanoparticles from Syzygium Cumini leaves extract with robust photocatalysis applications," *J. Mol. Liq.*, vol. **335**, 2021, doi: 10.1016/j.molliq.2021.116567.

[32] A. R. Malik *et al.*, "Green synthesis of RGO-ZnO mediated Ocimum basilicum leaves extract nanocomposite for antioxidant, antibacterial, antidiabetic and photocatalytic activity," *J. Saudi Chem. Soc.*, vol. **26**, no. 2, p. 101438, 2022, doi: 10.1016/j.jscs.2022.101438.

[33] M. Rafique *et al.*, "Novel Citrus aurantifolia leaves based biosynthesis of copper oxide nanoparticles for environmental and wastewater purification as an efficient photocatalyst and antibacterial agent," *Optik (Stuttg).*, vol. **219**, no. June, 2020, doi: 10.1016/j.ijleo.2020.165138.

[34] G. Parthasarathy, E. Arts, M. Venkatachalam, and E. Arts, "Characterization and Antibacterial activity of Green Synthesized ZnO Nanoparticles from Ocimum basilicum Leaf Extract A d v a n c e s i n B i o r e s e a r c h Characterization and Antibacterial activity of Green Synthesized ZnO Nanoparticles from Ocimum ," no. May, 2017, doi: 10.15515/abr.0976-4585.8.3.2935.

[35] A. S. Abdelsattar, W. M. Farouk, S. Mohamed Gouda, A. Safwat, T. A. Hakim, and A. El-Shibiny, "Utilization of Ocimum basilicum extracts for zinc oxide nanoparticles synthesis and their antibacterial activity after a novel combination with phage," *Mater. Lett.*, vol. **309**, no. November 2021, p. 131344, 2022, doi: 10.1016/j.matlet.2021.131344.

[36] M. Stan, A. Popa, D. Toloman, T. D. Silipas, and D. C. Vodnar, "Antibacterial and antioxidant activities of ZnO nanoparticles synthesized using extracts of Allium sativum, Rosmarinus officinalis and Ocimum basilicum," *Acta Metall. Sin. (English Lett.*, vol. **29**, no. 3, pp. 228–236, 2016, doi: 10.1007/s40195-016-0380-7.